Final Draft

of the original manuscript

Gavras, S.; Subroto, T.; Buzolin, R.H.; Hort, N.; Tolnai, D.:

The Role of Zn Additions on the Microstructure and Mechanical Properties of Mg–Nd–Zn Alloys.

In: International Journal of Metalcasting. Vol. 12 (2018) 3, 428 - 433.

First published online by Springer: 18.09.2017

https://dx.doi.org/10.1007/s40962-017-0174-3

THE ROLE OF Zn ADDITIONS ON THE MICROSTRUCTURE AND MECHANICAL PROPERTIES OF Mg-Nd-Zn ALLOYS

S. Gavras[1], T. Subroto[1], R.H. Buzolin[1,2], N. Hort[1], D. Tolnai[1].

[1]Magnesium Innovation Centre, Helmholtz-Zentrum Geesthacht, Max-Planck-Straße 1, Geesthacht, Germany.
[2]Graz University of Technology, Institute of Materials Science, Joining and Forming, Graz, Austria.

Keywords: Mg-Nd-Zn, phase identification, mechanical properties, synchrotron diffraction.

Abstract

Mg-rare earth alloys have improved yield strength and creep resistance compared to commercial alloys such as AZ91, AM60 or AS21. The influence of Zn additions on intermetallic phases and the resulting changes in the macroscopic mechanical behaviour of the materials, specifically Mg-Nd alloys, is not yet fully understood. The aim of this work is to identify the effect of Zn additions on the nature of the intermetallic phases and on the mechanical properties in a Mg-4Nd (wt.%) alloy. The addition of 8 wt.% Zn to a base Mg-4Nd wt.% alloy marginally improved the tensile and compression properties at room temperature or at 200°C with the exception of the 0.2% proof stress of Mg-4Nd-8Zn alloys when tensile or compression tested at 200°C. Two intermetallic phases, a quasi-binary $Mg_3(Zn,Nd)$ and ternary $Mg_{50}Nd_8Zn_{42}$, have been identified by the means of synchrotron diffraction and electron microscopy. These results indicate that there are some discrepancies in the current thermodynamic calculations, suggesting an update to the databases may be required.

Introduction

The addition of Zn to Mg-rare earth (Mg-RE) alloys has been shown to significantly improve mechanical properties including tensile and compression properties and elevated temperature creep resistance [1-4]. This means that by the addition of Zn to Mg-RE alloys lower concentrations of RE additions are required to achieve similar mechanical properties compared to Mg-RE alloys that do not have Zn additions. This is beneficial for the adoption of Mg-RE alloys for industrial applications such as in the automotive industry since RE elements are relatively expensive. It has been proposed that the addition of Zn to Mg-Nd alloys results in a reduction of the lattice parameter of the Mg-RE-Zn precipitates, from ~ 0.74 nm to ~ 0.72 nm [5]. Typically only relatively low concentrations of Zn (< 1.35 wt.%) are required to be alloyed with Mg-RE alloys such as Mg-Nd in order to detect an improvement in the alloy's mechanical properties [5]. However, there is no consistent description available in the literature as to which phases are present in the Mg-Nd-Zn system [6, 7]. In the current work, a binary Mg-4Nd wt.% alloy is compared with a ternary Mg-4Nd-8Zn wt.% in order to investigate the influence of Zn on the microstructure and mechanical properties. The use of such relatively high concentrations of Zn is used to help facilitate the formation of higher concentrations of intermetallic particles in order to assist with phase identification.

Experimental Procedure

The two alloys under investigation in the current work were Mg-4Nd wt.% and Mg-4Nd-8Zn wt.%, all alloy compositions in the current work will be presented in wt.%. The alloys were cast by permanent mould indirect chill casting producing cylinderical ingots with a length of 300 mm and diameter of 250 mm The casting process is described in greater detail elsewhere by [8]. Compositional analysis was measured via Spark-Optical Emission Spectroscopy (Spark-OES) using a Spectrolab M.

Tensile and compression samples were cut from ingots using Electron Discharge Machining (EDM). Tensile samples with a length of 60 mm were machined in order to have a gauge length of 35 mm and diameter of 6 mm with shoulder diameters of 9.8 mm. Compression samples had a length of 15 mm and a diameter of 10 mm. Tensile and compression tests were performed according to the DIN 50125 standard on a minimum of 5 samples per alloy and per condition. A Zwick-Z050 tensile and compression machine which has a maximum load of 50 kN was used at room temperature and at 200°C, using a strain rate of $10^{-3}s^{-1}$. Average grain size measurements were obtained via optical microscopy with an average of 100 grains measured per alloy using the line intercept method.

The microstructure was investigated using a TESCAN Vega3 Scanning Electron Microscope (SEM) in backscattered electron (BSE) mode. SEM samples were ground with SiC paper and polished using an oxide polishing suspension (OPS). Volume fraction analysis of intermetallic particles were determined by thresholding BSE micrographs of a minimum of 5 representative regions of the sample's microstructure. A measurement of the intermetallic (white threshold particles) was compared with the matrix (black threshold region). Characterisation of the intermetallic phases present in Mg-4Nd-8Zn was performed via selected area electron diffraction (SAED) on a Philips CM200 Transmission Electron Microscope (TEM) with accelerating voltage of 200 kV. TEM samples with diameter of 3 mm were ground to 150 μm and electropolished using a 1.5 % perchloric acid in ethanol solution. Bright field (BF) micrographs of the intermetallic particles were also obtained via TEM.

In situ synchrotron radiation experiments were carried out at the P07 beamline of Petra III, DESY (Deutsches Elektronen-Synchrotron). A monochromatic beam with the energy of 100 keV (λ = 0.0124 nm) and with a cross section of 1.1 mm x 1.1 mm was used. Diffraction patterns were recorded by a PerkinElmer 1622 flat panel detector (pixel size = $(200\ \mu m)^2$). The experiments were performed at room temperature. The morphology of the Debye-Scherrer rings was then analysed using the Fit2D® software. The diffraction patterns were then azimuthally integrated to obtain line profiles. The Pearson's crystallographic database (Release 2015/2016) and CaRIne crystallographic software (ver. 3.1) were used to calculate the theoretical diffraction patterns. The phases were identified by comparing the line profiles and the peak position in the database.

Results and Discussion

The compositions of the alloys used to determine tensile and compressive strength and also for microstructural analysis are shown in Table 1.

Table 1: Compositional measurements via Spark-Optical Emission Spectroscopy.

Composition	Nd wt.%	Zn wt.%
Mg-4Nd	4.20	0.00086
Mg-4Nd-8Zn	4.20	8.00

The representative stress-strain curves for the tensile tests are shown in Figure 1. The addition of 8wt.% Zn only marginally improved the tensile properties at room temperature (Figure 1a). This is also true for the tensile properties for the binary and ternary alloys compared at 200°C except for the 0.2% proof stress ($\sigma_{0.2}$) (Figure 1b). The addition of 8wt.%Zn decreases the $\sigma_{0.2}$ by approximately 13 MPa compared with the binary Mg-4Nd alloys when tensile tested at 200°C (Table 2).

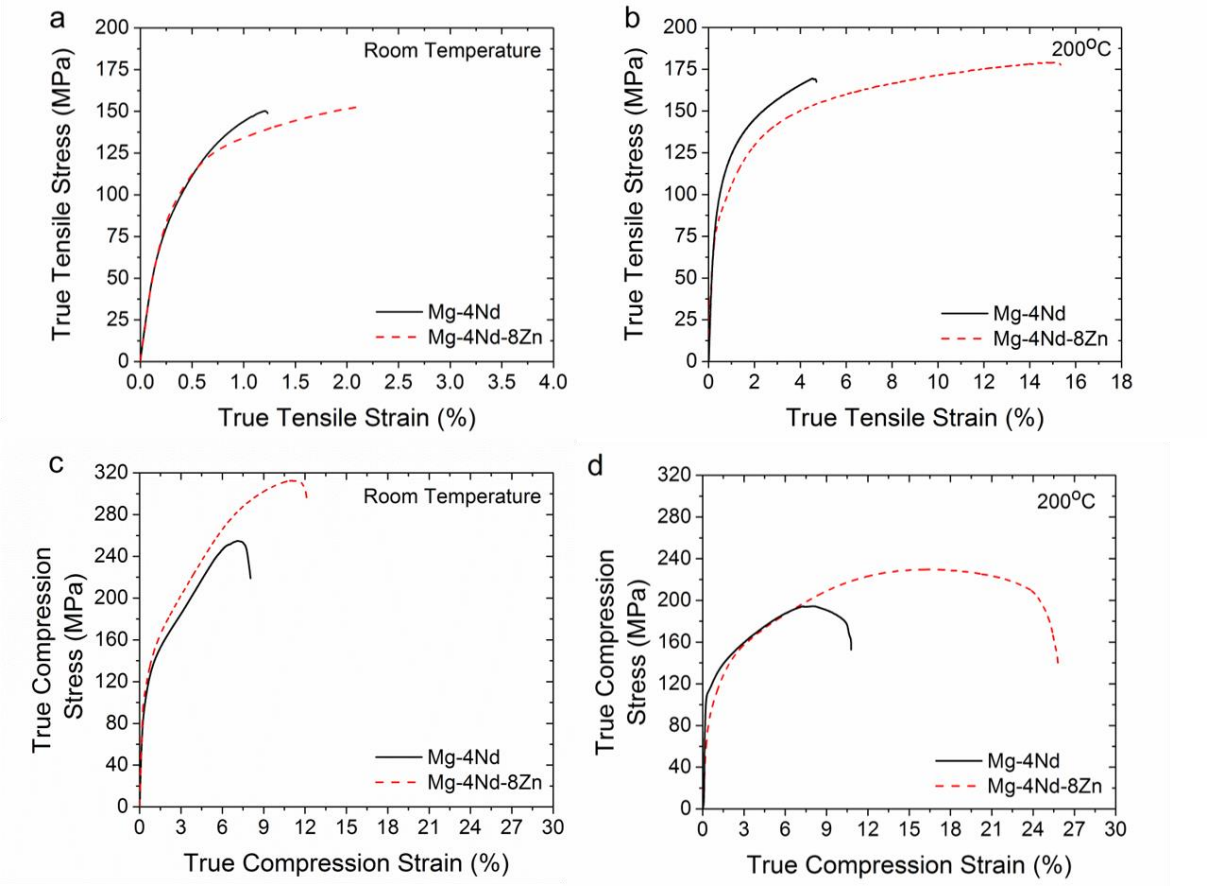

Figure 1: True stress-strain curves for Mg-4Nd and Mg-4Nd-8Zn tensile tested at a) room temperature and b) 200°C and compression tested at c) room temperature and d) 200°C.

A similar trend to the tensile properties is shown in relation to the compressive properties of Mg-4Nd and Mg-4Nd-8Zn (Figure 1c-d). There is a marginal improvement to the compression properties following the addition of 8wt.% with the exception of the $\sigma_{0.2}$ of the Mg-4Nd-8Zn alloy tested at 200°C in comparison to the Mg-4Nd alloy. At both room temperature and 200°C compression testing the addition of 8wt.% Zn improves all compression properties except for the compressive $\sigma_{0.2}$ of Mg-4Nd-8Zn at 200°C. The addition of 8wt.%Zn decreases the compressive $\sigma_{0.2}$ by approximately 10 MPa compared with the binary Mg-4Nd alloy (Table 2).

Table 2: Average tensile and compression properties of Mg-4Nd and Mg-4Nd-8Zn at room temperature and 200°C.

Average Tensile Properties				
Alloy (wt.%)	Test Temperature	$\sigma_{0.2}$ ±SD (MPa)	UTS ±SD (MPa)	Elong. (%) ±SD (MPa)
Mg-4Nd	Room Temp.	103.4 (±1.8)	147.7 (± 17.0)	1.2 (± 0.3)
Mg-4Nd-8Zn	Room Temp.	105.1 (±1.9)	151.4 (± 2.1)	2.0 (± 0.1)
Mg-4Nd	200°C	96.8 (± 2.1)	169.3 (± 12.1)	4.9 (± 1.3)
Mg-4Nd-8Zn	200°C	83.9 (±3.2)	177.7 (± 4.7)	15.2 (± 0.5)
Average Compression Properties				
Alloy (wt.%)	Test Temperature	$\sigma_{0.2}$ ±SD (MPa)	UCS ±SD (MPa)	Comp. (%) ±SD (MPa)
Mg-4Nd	Room Temp.	103.2 (± 5.0)	257.4 (± 11.3)	8.3 (± 0.7)
Mg-4Nd-8Zn	Room Temp.	115.0 (± 1.6)	311.9 (± 4.4)	13.0 (± 1.7)
Mg-4Nd	200°C	99.5 (± 7.1)	198.8 (± 13.1)	10.2 (± 1.0)
Mg-4Nd-8Zn	200°C	89.0 (± 0.4)	230.1 (± 0.3)	26.4 (± 1.0)

BSE micrographs are shown in Figure 2 highlighting the morphology and distribution of the intermetallic phases present in each alloy. The morphology of the intermetallic phase present in Mg-4Nd is continuous while for the Mg-4Nd-8Zn alloy there are two distinct intermetallic morphologies present, a semi-continuous intermetallic and a lamellar intermetallic phase. The increased elongation and compression properties of the Mg-4Nd-8Zn is likely related to the difference of intermetallic morphology between the two alloys. The combination of a semi-continuous intermetallic morphology and a lamellar eutectic morphology may inhibit the propagation of cracks through the interdendritic regions of the alloys. This would be less likely to occur in Mg-4Nd since it has a single, more continuous intermetallic morphology at the interdendritic regions, which facilitates crack propagation more easily than in the Mg-4Nd-8Zn alloy (Figure 2).

The average grain size of Mg-4Nd is larger than Mg-4Nd-8Zn and there is an expected increase in volume fraction of intermetallic from Mg-4Nd to Mg-4Nd-8Zn (Table 3).

Table 3: Average grain size and volume fraction of intermetallic particles present in Mg-4Nd and Mg-4Nd-8Zn.

Alloy (wt.%)	Ave. Grain Size (mm) ± SD	Ave. Vol. Frac. (%) Intermetallic ± SD
Mg-4Nd	0.36 ± 0.02	13.4 ± 0.4
Mg-4Nd-8Zn	0.20 ± 0.02	15.2 ± 0.7

The intermetallic phase present in the binary Mg-Nd alloys has been shown to be $Mg_{12}Nd$ [9, 10]. Mg-Nd hydrides [11] can also be observed in the binary Mg-4Nd alloy as relatively small white features (as observed in SEM BSE) predominantly near the intermetallic/α-matrix boundary (Figure 2b). The Mg-4Nd-8Zn has a lamellar eutectic and a semi-continuous intermetallic phase present at the dendrite boundaries.

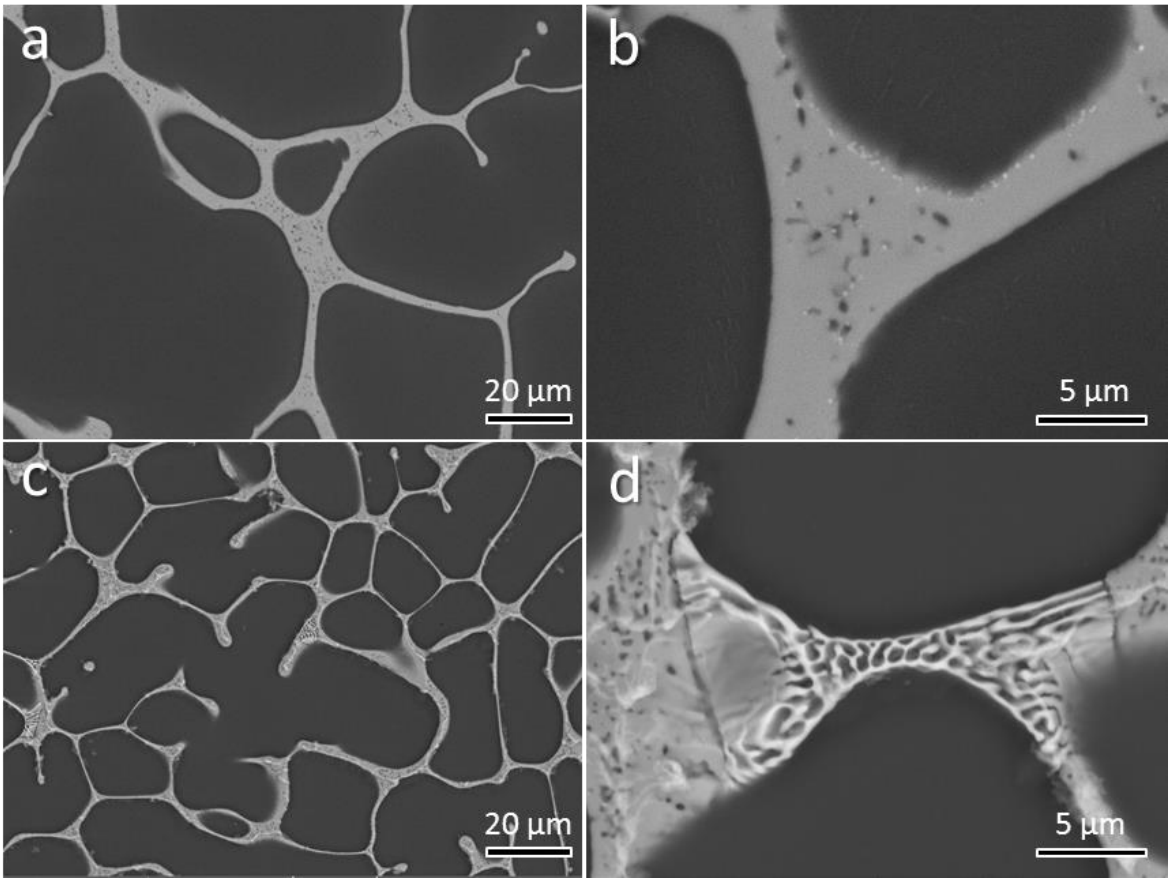

Figure 2: Backscattered electron micrographs of as-cast a-b) Mg-4Nd and c-d) Mg-4Nd-8Zn.

In order to identify if the intermetallic particles in Mg-4Nd-8Zn with differing morphologies are two distinct phases TEM diffraction analysis is performed. Figure 3 shows bright field TEM micrographs of the semi-continuous (Figure 3a) and the lamellar intermetallic particles (Figure 3b) with their corresponding SAED patterns. Following diffraction pattern analysis the semi-

continuous intermetallic is characterised as a c-centred orthorhombic ternary phase, $Mg_{50}Nd_8Zn_{42}$, while the lamellar intermetallic is face-centred cubic quasi-binary phase, $Mg_3(Nd,Zn)$.

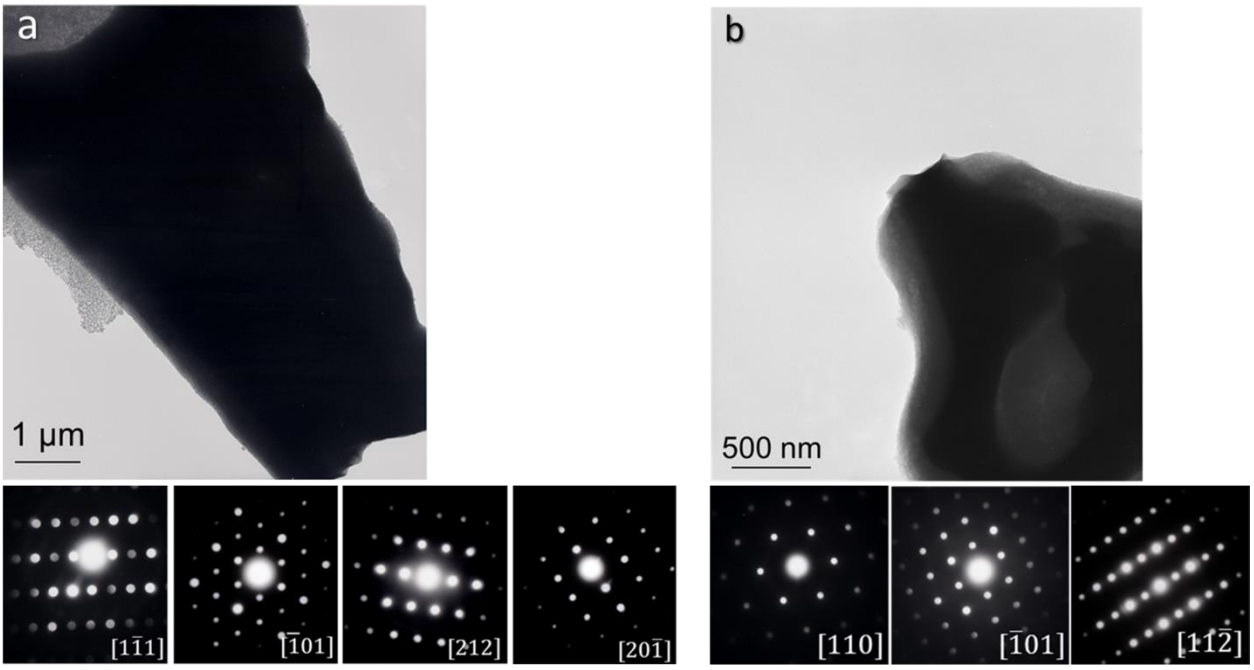

Figure 3: Bright field TEM micrographs with selected area electron diffraction patterns for a) c-centred orthorhombic and b) FCC phases present in Mg-4Nd-8Zn.

The synchrotron diffraction line profiles (Figure 4) confirm that the intermetallic present in Mg-4Nd alloy is $Mg_{12}Nd$ and in Mg-4Nd-8Zn are $Mg_{50}Nd_8Zn_{42}$ and $Mg_3(Nd,Zn)$.

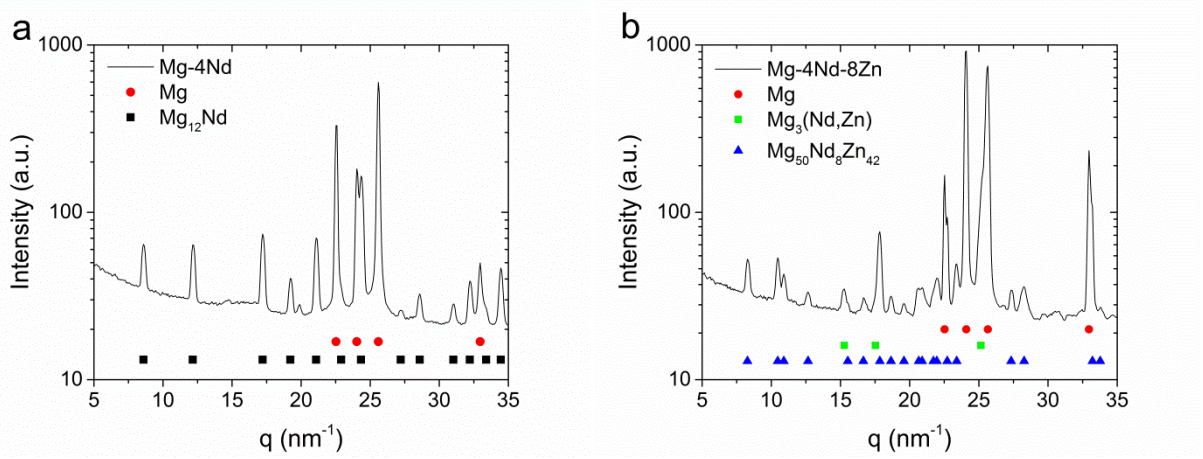

Figure 4: Synchrotron diffraction line profiles for a) Mg-4Nd and b) Mg-4Nd-8Zn.

There is however some disagreement between the results of the confirmed phases as identified by TEM diffraction analysis and the synchrotron diffraction line profiles in the Mg-4Nd-8Zn alloy with the currently accepted Mg-Nd-Zn ternary phase diagram. In the quasi-binary phase diagram

of the Mg-Nd-Zn system at 4 wt.% Nd only one intermetallic phase $Mg_{50}Nd_8Zn_{42}$ and α-Mg are shown to be present upon solidification at concentrations of 8 wt.% Nd (Figure 5). Both the TEM analysis and synchrotron diffraction analysis clearly indicate that a quasi-binary Mg_3(Zn, Nd) FCC phase forms at dendrite boundaries in addition to the c-centred orthorhombic phase $Mg_{50}Nd_8Zn_{42}$.

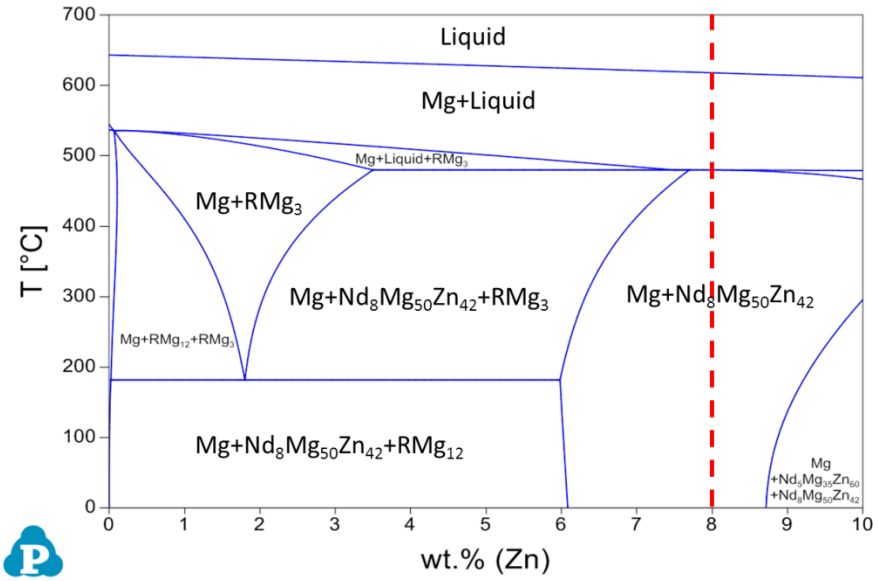

Figure 5: Quasi-binary phase diagram section of the Mg-Nd-Zn system at 4 wt.% Nd. The dashed line indicates the region of interest for the Mg-4Nd-8Zn alloy.

In previous investigations by Huang *et al.* [6], Xu *et al.* [7] and Pelton *et al.* [12] some inconsistencies between the stated phases in the Mg-Nd-Zn system are present. In the current work it is demonstrated that corrections to the existing ternary phase diagram of the Mg-Nd-Zn system are required. Further work with various concentrations of Zn is currently in progress which will help to confirm if any additional corrections are required.

Conclusions

The addition of 8 wt.% Zn to a base Mg-4Nd wt.% alloy marginally improved the tensile and compression properties at room temperature or at 200°C with the exception of $\sigma_{0.2}$ of Mg-4Nd-8Zn alloys when tensile or compression tested at 200°C. The addition of the relatively high concentration of Zn to the base Mg-4Nd alloy allowed for the identification of two intermetallic phases, a quasi-binary face centred cubic Mg_3(Zn,Nd) phase and a ternary c-centred orthorhombic $Mg_{50}Nd_8Zn_{42}$ phase. This result does not agree with the current ternary phase diagram for the Mg-Nd-Zn system which indicates that only a single intermetallic ternary phase should be present in a Mg-4Nd-8Zn alloy. Investigations into Mg-4Nd-xZn alloys will be conducted in order to further investigate the Mg-Nd-Zn ternary phase diagram.

Acknowledgements

The authors acknowledge the Deutsches Elektronen-Synchrotron for the provision of facilities within the framework of the Proposal I-20150471 and the Deutsche Forschungsgemeinschaft for the funding in the framework of the Proposals TO817/4- 1 and ME4487/1-1.

References

[1] D. Choudhuri, D. Jaeger, M.A. Gibson, and R. Banerjee, Scripta Materialia, Vol. 86, p. 32 (2014).
[2] C.J. Bettles, M.A. Gibson, and S.M. Zhu, Materials Science and Engineering A, Vol. A505, p. 6 (2009).
[3] M.A. Gibson, M. Easton, V. Tyagi, M. Murray, and G. Dunlop: Magnesium Technology, (2008), p. 227.
[4] *Magnesium elektron datasheet 463*.
[5] J.F. Nie, Metallurgical and Materials Transactions A: Physical Metallurgy and Materials Science, Vol. 43A, p. 3891 (2012).
[6] M. Huang, H. Li, H. Ding, Z. Tang, R. Mei, H. Zhou, R. Ren, and S. Hao, Journal of Alloys and Compounds, Vol. 489, p. 620 (2010).
[7] H. Xu, J. Fan, H.-L. Chen, R. Schmid-Fetzer, F. Zhang, Y. Wang, Q. Gao, and T. Zhou, Journal of Alloys and Compounds, Vol. 603, p. 100 (2014).
[8] F.R. Elsayed, N. Hort, M.A. Salgado Ordorica, and K.U. Kainer: Materials Science Forum. Trans Tech Publ, (2011), p. 65.
[9] D. Tolnai, C. Mendis, A. Stark, G. Szakács, B. Wiese, K. Kainer, and N. Hort, Materials Letters, Vol. 102, p. 62 (2013).
[10] M.A. Easton, M.A. Gibson, D. Qiu, S.M. Zhu, J. Gröbner, R. Schmid-Fetzer, J.F. Nie, and M.X. Zhang, Acta Materialia, Vol. 60, p. 4420 (2012).
[11] S. Zhu, J. Nie, M. Gibson, and M. Easton, Scripta Materialia, Vol. 77, p. 21 (2014).
[12] Z. Zhu, M.A. Gharghouri, and A.D. Pelton, The Journal of Chemical Thermodynamics, Vol. 94, p. 43 (2016).